Research Article | Vol. 32, No. 8 / 8 Apr 2024 / Optics Express 13450
Optics EXPRESS

Miniature atom bottle traps enabled by chiral doughnut light

VASILEIOS E. LEMBESSIS,[1] KORAY KOKSAL,[2] MOHAMED BABIKER,[3] AND JUN YUAN[3,*]

[1]Quantum Technology Group, Department of Physics and Astronomy, College of Science, King Saud University, Riyadh 11451, Saudi Arabia
[2]Physics Department, Bitlis Eren University, Bitlis 13000, Turkey
[3]School of Physics, Engineering and Technology, University of York, YO10 5DD, UK
[*]jun.yuan@york.ac.uk

Abstract: We highlight what we believe to be a novel optical set-up which enables the confinement of cold atoms in a finite set of sub-wavelength bottle traps. This involves two counter-propagating vortex beams with the same winding number $\ell = \pm 1$ and the same circular polarization ($\sigma = \mp 1$). Strong focusing generates significant longitudinal field components which become responsible for an on-axis standing wave enabling the axial confinement of far blue-detuned atoms. The off-axis radial confinement is provided by the optical potential due to the transverse components of the light. The trap characteristics are illustrated using experimentally accessible parameters and are tunable by changing the power, focusing and ellipticity of the light. Atoms trapped in such a set-up are useful for applications, including quantum simulation and quantum information processing.

1. Introduction

Optical vortex beams came to the fore in 1992 when Allen et al [1] showed that the photons of a Laguerre-Gaussian (LG) mode carry a quantized orbital angular momentum (OAM), $\ell\hbar$, pointing along the propagation direction. Here, ℓ is the so-called winding number. Today, optical vortex modes comprise a large family of coherent light beams, with the LG set and the Bessel set of modes being the most prominent members [2]. The emergence of the area of optical vortices stimulated huge theoretical and experimental investigations involving a very broad range of fields, from mechanical effects on atoms and on small particles [3,4,6,11], to quantum communications [13].

The fact that the photons of an optical vortex beam carry both linear momentum and orbital angular momentum lent a fresh boost to the physics of mechanical effects of light on atoms and small particles [3–13]. Optical vortex fields are not only capable of exerting forces and thus affect the translational motion of a particle but they can also exert a torque on it and can thus change its rotational motion around the beam propagation axis. Optical vortices have amplitude and phase functions with very rich spatial structures. The helicoidal phase fronts which are characteristic of these beams are inherently related to a zero intensity at all points on the axis in the paraxial regime. Their spatially dependent intensity profile can be exploited for blue-detuned ($\Delta>0$) and red-detuned ($\Delta<0$) optical dipole trapping of atoms in optical configurations with a cylindrical symmetry around the beam axis. Here, $\Delta = \omega - \omega_0$ is the difference between the angular frequency of the light (ω) and that of the atomic resonance (ω_0, also called Rabi frequency). They can form various novel optical environments such as those for the optical Ferris wheel (OFW) [14] in two dimensions and the helical optical tube (HOT) in three dimensions [15].

#516270 https://doi.org/10.1364/OE.516270
Journal © 2024 Received 20 Dec 2023; revised 9 Feb 2024; accepted 18 Feb 2024; published 27 Mar 2024

Optics EXPRESS

Among the different trapping configurations is the so-called bottle beam configuration which ensures a dark three-dimensional region in the shape of a bottle surrounded by light. In this region atoms can be trapped using blue detuning which ensures a very low photon scattering rate and a coherence time of the atoms that can reach up to several seconds compared to a red-detuned bottle trap centered on the bright regions.

The first bottle beam configuration was suggested and realised by Arlt and Padgett [16]. They used a computer-generated hologram to generate a superposition of two Laguerre–Gaussian modes, with zero winding number, such that the two beams interfere destructively to give rise to a (dark) beam focus which is surrounded in all directions by regions of higher intensity. Thus such an optical environment can be exploited for the blue detuned trapping of atoms. In 2009 Isenhower et al [17] demonstrated such an optical bottle beam in which they managed to trap Cs atoms. Their atom trap was created by the interference of two Gaussian beams with different waists which created a harmonic potential only along the axial direction. In 2010 Xu et al [18] demonstrated the trapping of a single Rb atom in an optical bottle beam trap formed by a strongly focused blue-detuned laser beam, which passes through a computer-generated phase hologram imprinted on a spatial light modulator. In 2012 Arnold used blue-detuned counter-propagating Laguerre-Gaussian beams to localise ultra-cold atoms in dark regions [19]. In 2014 a theoretical investigation of the trapping properties of the bottle beam created by Arlt and Padgett was reported [20]. With the bottle trap boundaries defined by the light intensity maxima, the trapping region was estimated to have an axial spatial size of around 40 μm ($\approx 52\lambda$), while the radial trapping size was around 6 μm ($\approx 7.8\lambda$). In 2012 Li et al [21] demonstrated the trapping of single Cs atoms in a bottle beam trap created by crossing two vortex beams. We note that all the aforementioned bottle trapping schemes had only a single bottle-like trapping region. In 2020 Baredo and colleagues managed to create two such traps 40μm apart to study the dipole-dipole coupling between individual Rydberg atoms using a holographic method [22]. These traps provided a harmonic potential only in the axial direction. In 2021, Xiao et al. compared different schemes for the generation of bottle beams used in tweezing experiments [23]. However, none of those schemes managed to demonstrate trapping in sub-wavelength dimensions.

It is well known that the total angular momentum of a coherent paraxial light beam consists of two parts, the OAM and the spin angular momentum (SAM). The latter is related to the two types of circular polarizations, namely counter-clockwise and clockwise. Recent work has pointed out that as the beam focusing becomes stronger, longitudinal components of the electric and the magnetic fields can be comparable in magnitude to transverse components [24–27]. When the beam carries a SAM the longitudinal components become responsible for the appearance of a new term in the beam intensity in which the OAM is coupled to the SAM. This term displays a sensitivity to the chirality of the circularly-polarized input beams since it reverses sign when either OAM or SAM reverses sign. Under such conditions a strongly focused optical vortex beam can generate optical dipole traps for atoms the characteristics of which depend crucially on the beam properties [28].

This paper is concerned with optical traps involving twisted light in which the longitudinal field components and the spin-orbit coupling play important roles. We aim to uncover the trapping properties of the standing wave created by two counter-propagating strongly focused optical vortices with winding numbers of the same magnitude and sign and the same circular polarization. Our work shows that the intensity of this light field configuration, when the common winding number is either $\ell = +1$ or $\ell = -1$ is characterized by a set of dark trapping potential wells of sub-wavelength sizes with bottle-like three-dimensional shapes and so these regions can be exploited for atom trapping in the dark. Significantly the characteristics of the trapping regions as optical dipole traps for atoms are also tunable simply by the chirality of the optical vortex beams as well as by other beam parameters.

Optics EXPRESS

This article is organised as follows. In section 2 we specify the electric field associated with the two counter-propagating vortex beams, emphasising the role of the longitudinal field components which come into play under strong focusing. We consider in particular a Laguerre-Gaussian beam configuration and proceed to evaluate the intensity distribution which is proportional to the square of the modulus of the electric field vector. We identify the physical significance of the different terms, and single out for special consideration a term, which arises entirely due to having included the longitudinal field components. We point out that this term signifies the presence of spin-orbit coupling. This is a special feature of the optical field in which it displays chiral-sensitivity in the sense that any change of the sign of either the common winding number ℓ, or the sign of the circular polarisation σ leads to different results. In section 3 we consider the interaction of the two-level atom with the vortex field created by the two beams. We evaluate the Rabi frequency, assuming that the atom is blue-detuned and from the Rabi frequency we deduce the trapping potential experienced by the two-level atom immersed in the optical field. Analysis of the trapping potential in section 4 reveals that it consists of a number of quantum wells in the shape of three dimensional bottle traps. The special features of these traps are analysed further, pointing out that it is the additional confinement due to the longitudinal field component that led to the realisation of the bottle trap so that the atom faces deep potential walls in all three directions and the size of each trap is unusually small (typically under a wavelength). Assuming experimentally accessible parameters we illustrate the orders of magnitude involved in the depth of the trap and its quantum features, including an estimate of the tunneling rate between adjacent trapping sites (details of trap characteristics are listed in Table 1 and Table 2 of Appendix C). Section 5 considers the tunability of the depth of the bottle traps as well as their use in creating atom transport mechanisms. Section 6 contains a summary and discusses the features and results of this work. We suggest that the main findings should be followed by experimental work on the trapping of cold atoms in these miniature traps.

2. Optical vortex field

The optical environment is created by two counter-propagating Laguerre-Gaussian (LG) beams, labelled 1 and 2. Both have the same frequency ω and with winding numbers $\ell_1 = \ell_2 = \ell$, with the beams 1 and 2 also denoted by $(\pm)$ propagating along the $\pm z$ direction. The polarization of the transverse components of the light beams is represented by two complex numbers α and β. The individual electric fields are as follows [29]

$$\overrightarrow{E}_{\pm}(\rho,\phi,z,t) = \frac{1}{2}\left\{\alpha\mathcal{E}_{\pm}\hat{x} + \beta\mathcal{E}_{\pm}\hat{y} \pm \frac{i}{k}\left(\alpha\frac{\partial\mathcal{E}_{\pm}}{\partial x} + \beta\frac{\partial\mathcal{E}_{\pm}}{\partial y}\right)\hat{z}\right\} e^{\pm ikz - i\omega t}. \tag{1}$$

For circular polarisation, the complex numbers are $\alpha = 1/\sqrt{2}$ and $\beta = \pm i/\sqrt{2}$ and are such that

$$|\alpha|^2 + |\beta|^2 = 1; \quad \sigma = i(\alpha\beta^* - \alpha^*\beta) = \pm 1, \tag{2}$$

and $\mathcal{E}_{\pm}$ are the electric field amplitudes of the two counter-propergating waves and are given by

$$\mathcal{E}_{\pm} = \mathcal{E}_0 u(\rho,z) e^{i\ell\phi} e^{\pm i\Theta(\rho,z)}, \tag{3}$$

with $u(\rho,z)$ the common amplitude function. For the LG beams, this is given by [11,30]

$$u(\rho,z) = \frac{C_{|\ell|,p}}{\sqrt{1+z^2/z_R^2}}\left(\frac{\rho\sqrt{2}}{w_0\sqrt{1+z^2/z_R^2}}\right)^{|\ell|} \exp\left[-\frac{\rho^2}{w_0^2(1+z^2/z_R^2)}\right] L_p^{|\ell|}\left\{\frac{2\rho^2}{w_0^2(1+z^2/z_R^2)}\right\}, \tag{4}$$

and $\Theta(\rho,z)$ is the part of the phase functions which includes the Gouy and the curvature phases:

$$\Theta(\rho,z) = -(2p+|\ell|+1)\arctan\left(\frac{z}{z_R}\right) + \frac{kz\rho^2}{2(z^2+z_R^2)}. \tag{5}$$

Optics EXPRESS

Here w_0 is the beam waist, $z_R = w_0^2 k/2$ is the Rayleigh range, $C_{|\ell|,p} = \sqrt{p!/(p+|\ell|)!}$ and $L_p^{|\ell|}$ the associated Laguerre polynomial.

The above equations are based on the paraxial approximation for the transverse components, but have been improved upon by the inclusion of the longitudinal components which becomes important for strongly focused beams. However, we restrict ourselves to the case $(kw_0)^{-1}<1$ which amounts to $w_0>\lambda/(2\pi) \approx 0.16\lambda$, so the above expressions are still valid for the waist parameter we choose below ($w_0 = 0.9\lambda$, or NA$=\lambda/(\pi w_0)=0.35$) and there is no need to invoke the full non-paraxial correction.

As outlined in Appendix A, for circularly-polarised optical vortex modes, the longitudinal ($z-$) component of the electric field in Eq. (1) can be expressed in terms of cylindrical coordinates as follows

$$\overrightarrow{E}_{\pm,z}(\rho,\phi,z,t) = \pm\frac{i}{k}\left(\alpha\frac{\partial\mathcal{E}_\pm}{\partial x}+\beta\frac{\partial\mathcal{E}_\pm}{\partial y}\right)\hat{z}e^{\pm ikz-i\omega t} = \pm\frac{i}{\sqrt{2}k}e^{i\sigma\phi}\left(\frac{\partial}{\partial\rho}-\frac{\ell\sigma}{\rho}\right)\mathcal{E}_\pm\hat{z}e^{\pm ikz-i\omega t}. \quad (6)$$

Together with the $e^{i\ell\phi}$ phase factor in $\mathcal{E}_\pm$, the longitudinal component then has a total phase factor of $e^{i(\ell+\sigma)\phi}$. This is the well-known spin-to-orbital angular momentum conversion effect [31]. The two counter-propagating beams create a standing wave whose total electric field is given by:

$$\begin{aligned}\overrightarrow{E} &= \overrightarrow{E}_+ + \overrightarrow{E}_- \\ &= \mathcal{E}_0 e^{(i\ell\phi-i\omega t)}\cos(kz+\Theta)u\left[(\alpha\hat{x}+\beta\hat{y})+i\frac{\rho z}{(z^2+z_R^2)}(\alpha\cos\phi+\beta\sin\phi)\hat{z}\right] \\ &+ \mathcal{E}_0 e^{(i\ell\phi-i\omega t)}\frac{\sin(kz+\Theta)}{k}\left[-(\alpha\cos\phi+\beta\sin\phi)\frac{\partial u}{\partial\rho}-i\frac{\ell u}{\rho}(\beta\cos\phi-\alpha\sin\phi)\right]\hat{z}.\end{aligned} \quad (7)$$

The z- and ρ-dependence of the expression for Θ suggests that there is an effective wavelength defined by $k_{\text{eff}}z = kz - \Theta(\rho,z)$. This wavelength $\lambda_{eff} = 2\pi/k_{eff}$ not only depends on ℓ and p but also on ρ and its spatial variations explain the fact that the positions of the traps due to the standing wave are not exactly separated by $\lambda/2$ as we shall see below.

Consider now the modulus squared of the total field. Assuming that the LG modes are circularly-polarised, we make use of the identities $|\alpha| = |\beta| = 1/\sqrt{2}$, $\sigma = i(\alpha\beta^* - \alpha^*\beta) = \pm1$ and $\alpha\beta^* + \alpha^*\beta = 0$ to obtain for $|\overrightarrow{E}|^2$:

$$|\overrightarrow{E}|^2 = \mathcal{E}_0^2\left\{u^2\cos^2(kz+\Theta)\left[1+\frac{\rho^2z^2}{(z^2+z_R^2)^2}\right]+\frac{\sin^2(kz+\Theta)}{k^2}\left[\left(\frac{\partial u}{\partial\rho}\right)^2-2\frac{\sigma\ell u}{\rho}\frac{\partial u}{\partial\rho}+\frac{\ell^2u^2}{\rho^2}\right]\right\}. \quad (8)$$

Here u is the common amplitude function defined in Eq. (4). Thus $|\overrightarrow{E}|^2$ (and, hence, the light intensity of the system of two counter-propagating LG modes) consists of two terms; one proportional to $\cos^2(kz+\Theta)$ and another proportional to $\sin^2(kz+\Theta)$. This suggests that we have two standing waves with shifted maxima. The standing wave proportional to $\cos^2(kz+\Theta)$ is mainly due to the interference of the transverse components and this standing wave continues to exist in weak focusing conditions. The standing wave proportional to $\sin^2(kz+\Theta)$ is entirely due to the longitudinal field component and becomes significant when the magnitude of this field component increases under strong focusing conditions. In addition, the displaced maxima are also not exactly equally spaced because the effective wavelength of the light field now depends on both z and ρ.

3. Interaction with atoms

We are now in a position to consider the interaction of two-level atoms with the above mentioned field [32]. The two-level atom of mass M is characterised by its electric dipole moment $\overrightarrow{d}$,

Optics EXPRESS

its excitation energy $\hbar\omega_0$ and the natural width of its excited state Γ. Under far off-resonance conditions this interaction results in an optical dipole potential energy $\mathcal{U}$, which is proportional to the square of the Rabi frequency $\Omega = |\overrightarrow{d} \cdot \overrightarrow{E}|/\hbar$. We have for the potential $\mathcal{U}$:

$$\mathcal{U} = \frac{\hbar\Omega^2}{4\Delta} = \frac{\hbar\Omega_0^2}{4\Delta}\left\{u^2\cos^2(kz+\Theta)\left[1+\frac{\rho^2 z^2}{(z^2+z_R^2)^2}\right] + \frac{\sin^2(kz+\Theta)}{k^2}\left[(\frac{\partial u}{\partial \rho})^2 - 2\frac{\sigma\ell u}{\rho}\frac{\partial u}{\partial \rho} + \frac{\ell^2 u^2}{\rho^2}\right]\right\}, \tag{9}$$

where $\Delta = \omega - \omega_0$ is the detuning parameter and Ω_0 is the Rabi frequency associated with the field amplitude $\mathcal{E}_0$ of one of the two beams as $\Omega_0 = d\mathcal{E}_0/\hbar$. The Rabi frequency Ω is proportional to the total intensity of the light field according to $I/I_s = 2\Omega^2/\Gamma^2$, where I_s is the saturation intensity associated with the two-level transition and the intensity is proportional to $|\overrightarrow{E}|^2$.

Equation (9) describes the potential landscape presented to a two-level atom whose excitation frequency is blue-detuned from the frequency of the light. The significant new feature of this potential landscape is that the light is strongly focused so that the longitudinal field components of the LG modes are comparable to the transverse components. As pointed out earlier, the longitudinal field components introduce an additional standing wave. This standing wave is localised on the common beams' axis when $|\ell| = 1$, consistent with the requirement that $\ell + \sigma = 0$. The appearance of a spin-orbit coupling term endows the trapping potential landscape with the chirality-sensitive property. We shall show that the trapping potential wells are not just significantly deep, but constitute unusually small atom trapping regions of sub-wavelength dimensions.

4. Miniature atom bottle traps

A plot of the spatial variations of the optical dipole potential, Eq. (9), reveals an optical lattice landscape of peaks and troughs which exhibit dark regions of space surrounded by light and each of which has a bottle-like form. Thus each region can form a three dimensional trap for blue-detuned two-level atoms. To demonstrate this we find it convenient to use parameter values similar to those presented in the experiment by Isenhower et al. [17]. In their work, Isenhower et al. created the blue-detuned trap using two strongly focused Gaussian beams. One of their beams had a waist $w_1 = 0.94\lambda$ and the other had a waist $w_2 = 1.77\lambda$, where $\lambda = 532$nm (while the atomic transition wavelength $\lambda_0 = 852.35$nm). The resulting bottle trap had a trapping region with an axial (along z-axis) size of about 11.2λ and a radial one of about 3.76λ, a maximum axial intensity $8.8 \times 10^8\ Wm^{-2}$ and a maximum radial intensity $5.4 \times 10^8\ Wm^{-2}$.

Therefore, using parameters similar to those used by Isenhower et al. [17], we consider Cs atoms subject to an overall optical power of $P = 0.4$ mW which corresponds to a Rabi frequency $\Omega_0 = 3.6 \times 10^3\Gamma$. We assume equal beam waists $w_{0+} = w_{0-} = w_0 = 0.9\lambda$. Note that this is larger than $w_0 = 0.16\lambda$ (corresponding to $(kw_0)^{-1} = 1$), so the non-paraxial treatment is unnecessary. We focus on the Cs $6^2S_{1/2} - 6^2P_{3/2}$ transition of wavelength $\lambda_0 = 852.35$ nm and $\Gamma/2\pi = 5.18$ MHz. The laser light wavelength is $\lambda = 532$ nm, which corresponds to blue-detuning $\Delta = 1.33 \times 10^{15}$ Hz or $\Delta = 4.1 \times 10^7\Gamma$. Finally, the counter-propagating beams have a common winding number ℓ which can either be $\ell = +1$, or $\ell = -1$ for both beams.

In the first case when both beams have $\ell = +1$, $\sigma = -\ell = -1$ and using the parameters as stated above, we obtain the potential profile and contour plots shown in Fig. 1. We see that among the set of blue-detuned trap sites we have the first deep minimum at the origin $z = 0$, $\rho = 0$. This has an approximate harmonic potential form which arises by Taylor expansions of the potential about the point $z = 0$, $\rho = 0$. Retaining the leading term of such a three dimensional harmonic oscillator potential [33], we have:

$$\mathcal{U}(z=0,\rho=0) \approx \frac{1}{2}\mathcal{K}_{\rho,0}\rho^2 + \frac{1}{2}\mathcal{K}_{z,0}z^2, \tag{10}$$

Optics EXPRESS

where the spring constants have the values $\mathcal{K}_{\rho,0} = 9.32 \times 10^{-15}$ N/m and $\mathcal{K}_{z,0} = 2.38 \times 10^{-14}$ N/m respectively. A Cs atom trapped in this region has a ground state energy equal to $28E_{\rm rec}$. The potential energy has an off-axis saddle point with a depth equal to $60E_{\rm rec}$. The axial (along the z-axis) tunnelling rate is 0.0017 Hz while at the saddle point it is 0.038 Hz. The maximum restoring forces in this trap region are $F_{\rho,\max} = 6 \times 10^{-22}$N and $F_{z,\max} = 2 \times 10^{-21}$N. A Taylor expansion of the potential about the origin in terms of both ρ and z leads us to a relationship between the axial and radial spring constants as follows:

$$\mathcal{K}_{z,0} = \mathcal{K}_{\rho,0}\left(1 - \frac{2}{kz_R}\right)^2 (1-\sigma). \tag{11}$$

The spring constants become equal, i.e. $\mathcal{K}_{z,0} = \mathcal{K}_{\rho,0}$ for $\sigma = -1$ and $\ell = 1$ when $w_0 = 0.6\lambda$.

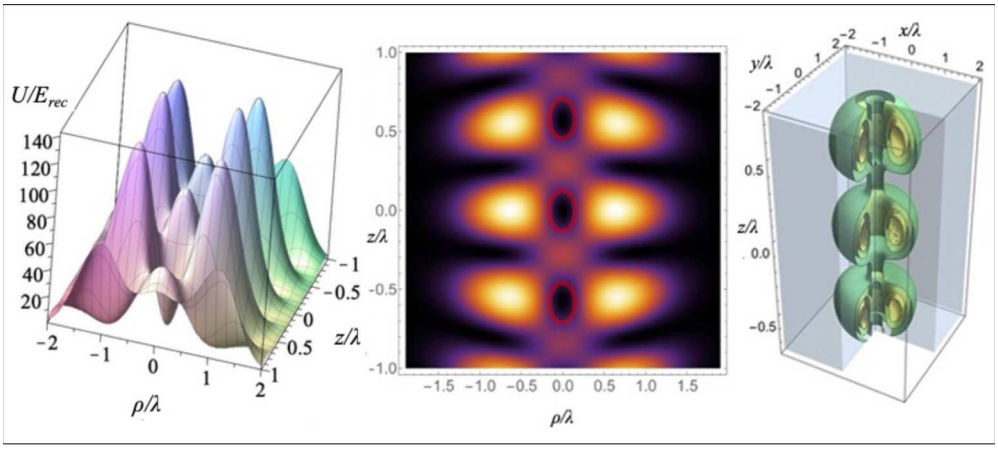

Fig. 1. The potential landscape (left panel) and contour plot (middle panel) of the bottle trapping potential (in recoil energy units $E_{\rm rec} = \hbar^2k^2/2M$) when both counter-propagating doughnut beams have $\ell = +1$ and $\sigma = -1$. Axes are scaled in wavelength units. In the contour plot, the potential represented by a gradient of colours ranging from black (minimum), through purple, red, orange, to white (maximum). The 3D bottle traps are highlighted with red ovals. The right panel shows the corresponding three dimensional trapping potential (with cutout to reveal the interior) for the on-axis trapping regions. The bottle traps are dark space bounded by the doughnut-shaped light pattern radially and by the off-setting standing wave light pattern on axis. See the main text for the parameter values used to generate these figures.

The adjacent on-axis minimum in Fig. 1 is at $z = 0.618\lambda$ and $\rho = 0$ and here, too, the potential has an approximate harmonic form given by:

$$\mathcal{U}(z = 0.618\lambda, \rho = 0) \approx \frac{1}{2}\mathcal{K}_{\rho,1}\rho^2 + \frac{1}{2}\mathcal{K}_{z,1}z^2, \tag{12}$$

where $\mathcal{K}_{\rho,1} = 7.03 \times 10^{-15}$ N/m and $\mathcal{K}_{z,1} = 1.92 \times 10^{-14}$ N/m. A Cs atom trapped in this region has a ground state energy equal to $25E_{\rm rec}$. The potential energy has an off-axis saddle point with a depth equal to $50E_{\rm rec}$. The axial (along the z-axis) tunnelling rate is 0.092 Hz while at the saddle point it is 0.238 Hz. The maximum restoring forces in this trap region are $F_{\rho,\max} = 5 \times 10^{-22}$N and $F_{z,\max} = 1.5 \times 10^{-21}$N.

The central trapping region has a characteristic axial size of about $\approx 0.6\lambda$ and a characteristic radial extent of about $\approx 1.2\lambda$, both defined as the peak-to-peak distance axially and twice the distance between the peak and the axis in the radial direction. The relative size cannot go below

Optics EXPRESS

0.5λ and this is a consequence of the fact that strong focusing amounts to a higher effective wavelength. The trapping volume of each of these bottle-like regions of the lattice is far smaller than the size of previously reported bottle traps [17,18,22,23]. In addition to the small size of the bottle traps, we see from Fig.1 (left panel) that the trap potential depth can be several hundreds of recoil energies for a modest input power. Thus this arrangement combines desirable features of an atom trap, namely a smaller trapping size, a deeper potential well and a negligible inter-well tunnelling; an ideal scenario for atomic spectroscopy which also, as we explain below, allows flexibly to tune the properties by adjusting the parameters, in order to probe several physically-interesting regimes.

In the second case when both beams have $\ell = -1$, we obtain a different potential profile as shown in Fig. 2 where the bottle trapping regions have disappeared and the potential, near the axis, has the form of a stack of doughnut trapping regions on the transverse plane. Note that the only change made is the reversal of the sign of the winding number. A similar result would be obtained if ℓ is kept the same but the sign of σ is reversed. The fact that we obtain different results merely due to a change in the sign of the winding number ℓ, or the sign of σ, is indicative of a chiral-sensitive behaviour. As we pointed earlier, this is entirely due to the presence of a strongly focused longitudinal field component. In this case, the spin-to-orbit conversion involved leads to $\ell + \sigma = -2$, i.e. a longitudinal component with topological charge of -2. In this case there is a vortex singularity on axis and the additional ρ dependent phase shift such as that due to beam divergence causes the interference light pattern due to the longitudinal field to merge with the interference light pattern due to the transverse components as shown in Fig. 2. It should be noted that the longitudinal trapping will not entirely disappear in the case of a linearly polarized light source for trapping because the linearly polarized light can be considered to be an equal superposition of light with $\sigma = 1$ and that with $\sigma = -1$. So the spin-to-orbit conversion mechanism still operates even for linearly-polarized light. But its contribution to the on-axis potential barrier is roughly reduced to a quarter of the fully circularly polarized ($\sigma = -1$) beam, because the amplitude of such beam is reduced by half as the other circularly polarized ($\sigma = 1$) component does not contribute to the on-axis electric field. For more details, see the comparison of the relevant trap characteristics in the last two columns of Table 1 of Appendix C.

Another equally interesting case arises when we consider that the counter-propagating LG beams have a non-zero radial index p, in which case there are $p + 1$ bright rings on the transverse plane. This has the following consequences. The bottle traps are still situated on the axis but now they are surrounded by torroidal (ring-like) trapping regions. The axial positions of these ring-like regions are shifted with respect to the axial positions of the bottle traps. Figure 3 displays the case in which $p = 1$, and $\ell = 1$.

In the harmonic approximation a cold atom of mass M in a given bottle trap is an anisotropic three dimensional harmonic oscillator possessing spring constants in both the radial and axial directions. Given that the corresponding harmonic oscillator frequencies are $\tilde{\omega}_x = \tilde{\omega}_y = \sqrt{\mathcal{K}_\rho/M}$, $\tilde{\omega}_z = \sqrt{\mathcal{K}_z/M}$, the quantum states of the atom in the bottle trap are formed as products of three one-dimensional harmonic oscillator wavefunctions. We have

$$\Psi_{\{n_i\}} = \prod_{i=x,y,z} [2^{n_i} n_i!]^{-\frac{1}{2}} \left(\frac{\alpha_i^2}{\pi}\right)^{\frac{1}{4}} e^{-\alpha_i^2 r_i^2/2} H_{n_i}(\alpha_i r_i), \tag{13}$$

where H_{n_i} are Hermite polynomials and the subscript $\{n_i\}$ stands for n_x, n_y, n_z, where $n_i \geq 0$ are integers; $\alpha_i^2 = M\tilde{\omega}_i/\hbar$, with $r_i = x, y, z$ and $\tilde{\omega}_i$ is the angular frequency of the harmonic oscillator along the $i-$axis. The corresponding energy eigenvalues are given as:

$$E_{n_x,n_y,n_z} = \sum_{i=x,y,z} \hbar\tilde{\omega}_i \left(n_i + \frac{1}{2}\right) = \hbar\tilde{\omega}_x \left(n_x + n_y + 1\right) + \hbar\tilde{\omega}_z \left(n_z + \frac{1}{2}\right). \tag{14}$$

Optics EXPRESS

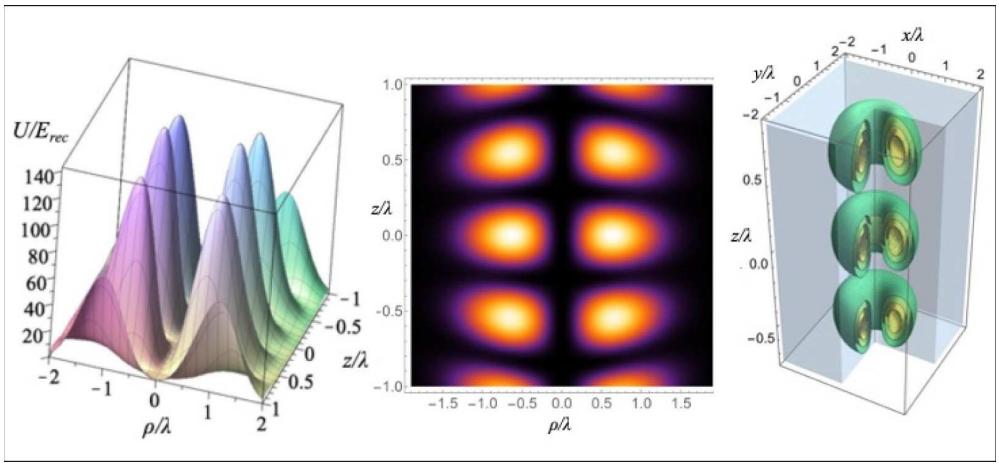

Fig. 2. The potential landscape (left panel) and contour plot (middle panel) of the bottle trapping potential (in recoil energy units $E_{\text{rec}} = \hbar^2 k^2/2M$) when both counter-propagating doughnut beams have $\ell = -1$ and $\sigma = -1$. Axes are scaled in wavelength units. In the contour plot, the potential represented by a gradient of colours ranging from black (minimum), through purple, red, orange, to white (maximum). The right panel shows the corresponding three dimensional trapping potential (with cutout to reveal the interior) for the on-axis trapping regions. We clearly see that the bottle trap regions exhibited in Fig. 1 do not exist in this case, as there is no light pattern to confine the atoms along the axis. See the main text for the parameter values used to generate these figures.

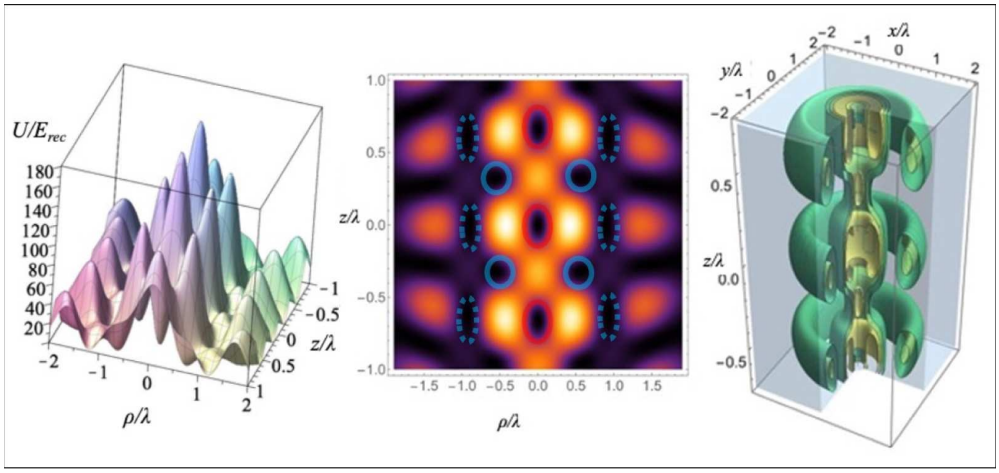

Fig. 3. The potential landscape (left panel) and contour plot (middle panel) of the bottle trapping potential (in recoil energy units $E_{\text{rec}} = \hbar^2 k^2/2M$) when both counter-propagating doughnut beams have $p = 1$, $\ell = 1$ and $\sigma = -1$. Axes are scaled in wavelength units. In the contour plot, the potential represented by a gradient of colours ranging from black (minimum), through purple, red, orange, to white (maximum). The 3D bottle traps are highlighted with red ovals. The secondary ring-like 3D traps are indicated by the blue circles and dashed blue ovals. The right panel shows the corresponding three dimensional trapping potential (with cutout to reveal the interior) for the on-axis trapping regions. We clearly see that the on-axis bottle trap regions are now accompanied by ring-like trapping regions. See the main text for the parameter values used to generate these figures.

Optics EXPRESS

The numerical examples we have shown concern very deep optical dipole potential where the trapped atoms are in the so-called Mott-insulator regime [34]. Deep atom trapping is prerequisite for achieving the so-called Lamb-Dicke limit which is ideal for atomic spectroscopy experiments on trapped atoms as well as for use in the generation of quantum collisional gates [35]. By reducing the intensity of the light fields we may have shallower bottle traps which allow tunneling of atoms between adjacent traps. Note that, as the figures indicate, the trapping region is, in general, ellipsoidal. The potential minima along the axial direction occur at different distances from the origin than those in the radial direction.

5. Discussion

The optical dipole trapping potentials we have demonstrated are of sub-wavelength dimensions mainly because the trapping is the result of an interference pattern arising from counter propagating vortex beams. The three dimensional trapping is achieved by the transverse beam components for the radial confinement and by the longitudinal field component for the axial confinement. The utility of this physical environment can be extended in different ways, as the following examples show [36].

5.1. Atom transport via moving traps

With a slight modification, the setup can be used for the coherent transport of trapped atomic samples in an optical conveyor belt. This case arises if the two LG modes have slightly different frequencies ω_1, ω_2, such that $\omega_1 - \omega_2 = \delta$. In this case the phase angle Θ which appears in Eq. (8) is replaced by $\Theta + \delta t/2$ and the resulting intensity pattern becomes time-dependent and, so, it moves in space [37]. Such a functionality can be used to perform a displacement of trapped atoms over a known distance [38].

5.2. Trap tunability

We have so-far demonstrated the optical potential for a set of parameters similar to those used in an earlier experiment [17] to highlight the feasibility of our approach. Focusing on our set of parameters, we now explain that some of these parameters can be modified to tune the trapping properties.

The simplest parameter to modify is the laser power. We have listed some examples of the resulting trap characteristics in Table 1 of Appendix C. The other parameter is the ellipticity of the polarisation of the trapping light, which can be varied from fully left-circularly-polarized light to fully right-circularly polarized light, providing fine control over the inter-trap axial interaction without affecting in a significant way the radial trapping characteristics. The use of elliptical light introduces a breaking down of cylindrical symmetry (see the general expression for the electric field expression in Eq. (7), but our simulation (see Appendix B) suggests that the resulting azimuthal dependence is negligible for the on-axis trapping potential and hence the on-axis trapping potential barrier height can be tuned from maximun (for $\sigma = -\ell = -1$) to zero (for $\sigma = \ell = 1$) smoothly by changing the ellipticity of the light source used. Following our analysis in Appendix B, a rough scaling relationship for on-axis potential barrier height with σ can be used for guidance: $U_{\text{axial-barrier-height}}(1{>}\sigma{>}-1) \sim |(1-\sigma)/2|^2 U_{\text{axial-barrier-height}}(\sigma = -1)$, assuming only $\sigma = -1$ circularly-polarized beam component contributes to on-axis potential barrier in our examples. In Table 1 of Appendix C, the characteristics of possible bottle traps for linear polarization are also given. As expected, the on-axis potential barrier is roughly 1/4 of the maximum on-axis (axial) barrier height when the correctly circularly-polarised light ($\sigma = -1$) is employed.

The third source of tunability control is the beam waist w_0 which can be easily adjusted to reduce the trapping depth and the tunnelling barrier, allowing the interaction strength to be increased for atoms trapped in the neighbouring bottle-shaped wells. The relationship between

Optics EXPRESS

the radial spring constant and the axial one is given by Eq. (11). This varies with the beam waist w_0 and we have explained that it is in principle possible to achieve an isotropic three dimensional harmonic trap at $w_0 = 0.6\lambda$. Interestingly, we find that the variation of the peak beam intensity with the waist parameter w_0 indicates that K_ρ is smaller than K_z for larger w_0. The relevant controlling parameters for the transverse field components are not only their intensities, but also the sizes of their spatial variations. While the diameter of the doughnut shape of the transverse field scales with the beam waist, the standing wave pattern of the longitudinal components are largely constrained to be always sub-wavelength in size.

Due to the variation of the barrier height surrounding the three dimensional bottle traps, the trap depth is defined by the minimum potential barrier at the saddle points. We have checked by explicit evaluations that as the beam waist increases from 0.9 λ (NA=0.35) to 1.3 λ (NA=0.25), the trap depth, measured as the lowest potential barrier height at the saddle point, changes from 600 recoil energies down to about 200 recoil energies. A similar scaling relationship with the beam waist exists for the tunnelling barriers between the bottle traps. For more details, see Table 2 of Appendix C. This flexibility provided by the adjustable parameters opens the door for the modification of the properties of the trapped atoms and their mutual interactions. For example, the atoms trapped can be tuned as Mott-like to superfluid, due to the significant change in the tunneling rates between central and its first nearest neighbour bottles.

5.3. Applications

The tunability of the miniature atomic bottle traps allows a range of cold atomic physics to be investigated. Here we briefly mention a few examples. At sufficiently strong focusing, trapped atoms can be in a Mott-insulator like state, with minimum tunnelling between the neighbouring traps. This allows atoms to be treated as isolated and this situation would be useful for high resolution spectroscopy [39]. As the on-axis trap barrier is lowered, one can adjust the strength of the coupling of the atoms in the neighbouring traps to study the processes of quantum tunnelling and quantum localization [43]. The conveyor-belt mechanism also allows the atomic potential to be modified adiabatically. The coupling of the atoms inside a doughnut ring-like trap with the atoms in the atomic bottle traps, as Fig. 3 indicates, raises the interesting possibility of studying magnetic coupling in the presence of a magnetic field. With ingenuity, we expect that the list of applications will be further expanded.

6. Conclusions

In conclusion, we have shown how a couple of strongly focused counter-propagating optical vortex beams with the same winding number, either $\ell = +1$ or $\ell = -1$ and the same circular polarisation, can generate a set of atom trapping quantum wells of bottle-like characters on-axis. This means that their intensity profile, along the beams' propagation axis is characterized by ellipsoidal dark regions surrounded by light. The depth of the quantum wells depends either on the sign of ℓ or the sign of σ. We have shown that the two cases yield different results, indicating that the optical environment generated by the two beams exhibits chirality.

We began by specifying the electric field associated with the two counter-propagating vortex beams, emphasising the role of the longitudinal field component which comes into play under strong focusing conditions. Our treatment conforms with the main criterion for the extent of focusing, namely that for tight focusing $(k_z w_0)^{-1}>1$. This amounts to $w_0<\lambda/(2\pi) \approx 0.16\lambda$. We chose $w_0 = 0.9\lambda$ which is much larger than 0.16λ, confirming the suitability of our formalism in dealing with the optical trap.

We concentrated on the case of Laguerre-Gaussian beams, taking full account of the spatial dependence in the Gouy and curvature phases and of the finiteness of the Rayleigh range z_R. We proceeded to evaluate the intensity distribution which is proportional to the square of the modulus of the electric field vector. We identified the different terms, and pointed out a term,

Optics EXPRESS

which arises entirely due to having included the longitudinal field components. This involves spin-orbit coupling which endows the field with chirality in the sense that any change of the sign of either the common winding number ℓ, or the sign of the circular polarisation σ leads to different results. The interaction of the two-level atom is in terms of the Rabi frequency which led us to the trapping potential. The trapping potential is found to consist of a number of quantum wells in the shape of three dimensional bottle traps. It is the additional confinement arising from the on-axis longitudinal field component that led to the realisation of the bottle traps so that the atom faces deep potential walls in all three directions and the size of each trap is unusually small (typically under a wavelength). Using experimentally accessible parameters we illustrated the orders of magnitude involved as regards the depth of the trap and its quantum features, including an estimate of the tunneling rate between adjacent trapping sites, which we found to be extremely small. This is because the optical dipole potential is very deep, so the trapped atoms are in the Mott-insulator regime [34]. We suggest that these findings should be followed by experimental work on cold atoms in these miniature traps.

It should be noted that the dipole trapping potential for atoms discussed here could also contribute to the gradient force trapping of particles whose electromagnetic response is dominated by strong resonance absorption and whose size is small (i.e. of the order of a 10th of the light wavelength, or smaller) as long as the dipole approximation assumed here is valid. Our simpler free-space interference approach complements the more sophisticated micro-engineered approaches based on metasurface optics [40], micro-optics [41] and diffraction from nanostructure [42], which can produce deep sub-wavelength 3D traps, but does require a quality focusing lens with a high numerical aperture.

The types of fields we have dealt with here, find useful application in dark atom trapping and also could act as an optical conveyor belt for trapped cold atom samples. In situations where a bichromatic field with large opposite detunings is set up we obtain the well-known form of a one-dimensional lattice but the potential depth and its topology depend entirely on the winding number and the polarization of the light field. The origin of these features due to this type of

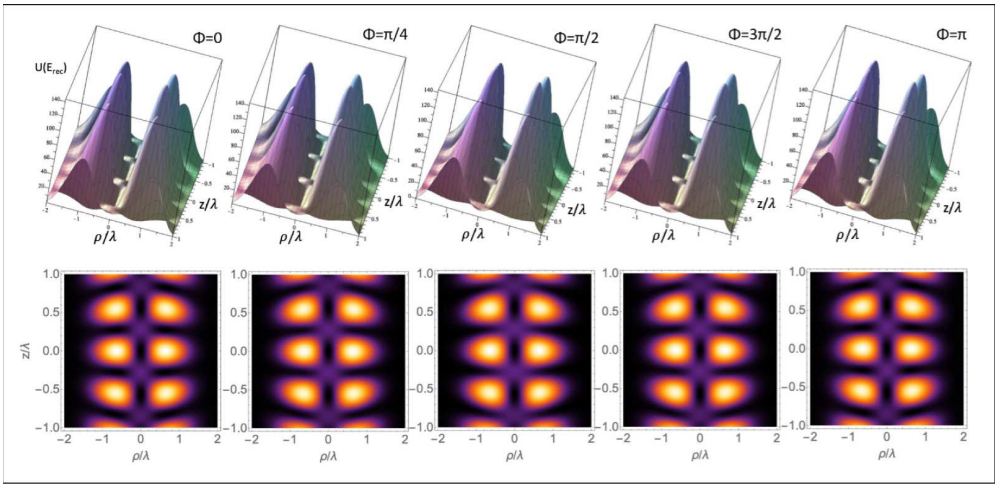

Fig. 4. The bottle trapping potential ($\mathcal{U}$, in recoil energy units $E_{\rm rec} = \hbar^2 k^2/2M$) when both counter-propagating doughnut beams are linearly-polarised along $\hat{x}$ and both have $p = 0$, $\ell = 1$. Distances along the axes are scaled in wavelength units. The potential for different ϕ-planes are shown as subplots either in pseudo-3D surface plots (the upper panels) or pseudo-color 2D plots (the lower panel) at different azimuthal planes. The other parameter values used here are the same as those used to generate the Figs. 1–3.

Optics EXPRESS

light fields is the existence of a longitudinal field component, which, in the case of circularly polarized light, is responsible for the coupling of light's OAM to SAM which is significant. The novel forms of the electromagnetic fields we have focused on here, Eq. (1), which we have used to unveil their utility in the trapping of atoms in miniature atom traps, could also be exploited in the study of the coherent mechanical effects of atoms, including atom diffraction in the Raman-Nath regime, the Bragg and Stern-Gerlach effect [44], as well as in the studies of the Kapitza-Dirac effect when atomic beams cross the standing light wave fields [45] and for the generation of ponderomotive potentials on electrons [46], but such issues will not be elaborated on any further here.

Although our concern here has been mainly with circularly-polarised counter-propagating beams, the question arises as to what kind of trapping one gets if both beams are in general elliptically polarised, including linearly-polarised. So we have considered this issue in Appendix B. We find that the potential in this case acquires dependence on the azimuthal angular variable ϕ. The potential for linear polarisation is displayed in Fig. 4 for different ϕ using the same parameters as for the circularly polarised case. We conclude that the bottle potential with linearly polarised beams is much reduced in comparison with the appropriately circularly-polarised case.

Appendix A: derivation of equation (6)

The first step in the derivation of Eq. (6) is to make use of the transformational relations:

$$\frac{\partial f}{\partial x} = \frac{\partial \rho}{\partial x}\frac{\partial f}{\partial \rho} + \frac{\partial \phi}{\partial x}\frac{\partial f}{\partial \phi} = \cos\phi\frac{\partial f}{\partial \rho} - \frac{\sin\phi}{\rho}\frac{\partial f}{\partial \phi}; \tag{15}$$

$$\frac{\partial f}{\partial y} = \frac{\partial \rho}{\partial y}\frac{\partial f}{\partial \rho} + \frac{\partial \phi}{\partial y}\frac{\partial f}{\partial \phi} = \sin\phi\frac{\partial f}{\partial \rho} + \frac{\cos\phi}{\rho}\frac{\partial f}{\partial \phi}, \tag{16}$$

given that $x = \rho\cos\phi$ and $y = \rho\sin\phi$. For the vortex beams given in Eq. (1), we have $\frac{\partial \mathcal{E}_\pm}{\partial \phi} = il\mathcal{E}_\pm$. We can now consider the relevant expression in the third term of Eq. (1), as follows:

$$\frac{i}{k}\left(\alpha\frac{\partial \mathcal{E}_\pm}{\partial x} + \beta\frac{\partial \mathcal{E}_\pm}{\partial y}\right) = \frac{i}{k}\left[(\alpha\cos\phi + \beta\sin\phi)\frac{\partial \mathcal{E}_\pm}{\partial \rho} + \frac{il}{\rho}(\beta\cos\phi - \alpha\sin\phi)\mathcal{E}_\pm\right]. \tag{17}$$

For circularly-polarized beams, $\alpha = 1/\sqrt{2}$, $\beta = i\sigma/\sqrt{2}$ where $\sigma = \pm 1$, we can then write

$$\frac{i}{k}\left(\alpha\frac{\partial \mathcal{E}_\pm}{\partial x} + \beta\frac{\partial \mathcal{E}_\pm}{\partial y}\right)_{cp} = \frac{i}{\sqrt{2}k}\left[(\cos\phi + i\sigma\sin\phi)\frac{\partial \mathcal{E}_\pm}{\partial \rho} + \frac{il}{\rho}(i\sigma\cos\phi - \sin\phi)\mathcal{E}_\pm\right], \tag{18}$$

where the subscript cp stands for circular polarisation. Finally, recognizing $i(i\sigma\cos\phi - \sin\phi) = -\sigma(\cos\phi + i\sigma\sin\phi)$, we have

$$\frac{i}{k}\left(\alpha\frac{\partial \mathcal{E}_\pm}{\partial x} + \beta\frac{\partial \mathcal{E}_\pm}{\partial y}\right)_{cp} = \frac{i}{\sqrt{2}k}\left[e^{i\sigma\phi}\frac{\partial \mathcal{E}_\pm}{\partial \rho} - \frac{l\sigma}{\rho}e^{i\sigma\phi}\mathcal{E}_\pm\right] = \frac{ie^{i\sigma\phi}}{\sqrt{2}k}\left[\frac{\partial \mathcal{E}_\pm}{\partial \rho} - \frac{l\sigma}{\rho}\mathcal{E}_\pm\right], \tag{19}$$

which leads us to the result in Eq. (6).

Another special case is that of linear polarization of the transverse components, for example, $\alpha = 1$ and $\beta = 0$, we have from Eq. (17),

$$\begin{aligned}\frac{i}{k}\left(\alpha\frac{\partial \mathcal{E}_\pm}{\partial x} + \beta\frac{\partial \mathcal{E}_\pm}{\partial y}\right)_{lp} &= \frac{i}{k}\left[(\cos\phi)\frac{\partial \mathcal{E}_\pm}{\partial \rho} + \frac{il}{\rho}(-\sin\phi)\mathcal{E}_\pm\right] \\ &= \frac{ie^{i\phi}}{2k}\left[\frac{\partial \mathcal{E}_\pm}{\partial \rho} - \frac{\ell}{\rho}\mathcal{E}_\pm\right] + \frac{ie^{-i\phi}}{2k}\left[\frac{\partial \mathcal{E}_\pm}{\partial \rho} - \frac{\ell(-1)}{\rho}\mathcal{E}_\pm\right],\end{aligned} \tag{20}$$

Optics EXPRESS

where the subscript *lp* stands for linear polarisation. This is consistent with the result for a pure circular polarization, but this time the longitudinal contribution is equally divided between left- and right-circularly polarized transverse components, as to be expected.

Appendix B: polarization effects

The case when our two counter-propagating beams are both linearly-polarised is a special but illuminating case. The corresponding dipole potential can be directly derived by taking the modulus-square of the electric field given in Eq. (7) and setting $\alpha = 1$ and $\beta = 0$, which correspond to linear polarisation along $\hat{x}$. We have for $\mathcal{U}$

$$\begin{aligned}\mathcal{U} = \frac{\hbar\Omega_0^2}{4\Delta}\Bigg\{ & u^2\cos^2(kz+\Theta)\left[1+\frac{\rho^2 z^2\cos^2\phi}{(z^2+z_R^2)^2}\right] \\ & + \frac{\sin^2(kz+\Theta)}{k^2}\left[(\frac{\partial u}{\partial\rho})^2\cos^2\phi + \frac{\ell^2 u^2}{\rho^2}\sin^2\phi\right] \\ & + \sin[2(kz+\Theta)]\frac{u^2 z\ell}{4k(z^2+z_R^2)}\sin 2\phi\Bigg\}.\end{aligned} \tag{21}$$

As $\cos^2\phi = (1+\cos 2\phi)/2$ and $\sin^2\phi = (1-\cos 2\phi)/2$, we have:

$$\begin{aligned}\mathcal{U} = \frac{\hbar\Omega_0^2}{4\Delta}\Bigg\{ & u^2\cos^2(kz+\Theta)\left[1+\frac{\rho^2 z^2}{2(z^2+z_R^2)^2}\right] \\ & + \frac{\sin^2(kz+\Theta)}{2k^2}\left[(\frac{\partial u}{\partial\rho})^2 + \frac{\ell^2 u^2}{\rho^2}\right] \\ & + \sin[2(kz+\Theta)]\frac{u^2 z\ell}{4k(z^2+z_R^2)}\sin 2\phi \\ & + \cos^2(kz+\Theta)\left[\frac{\rho^2 z^2}{2(z^2+z_R^2)^2}\right]\cos 2\phi \\ & + \frac{\sin^2(kz+\Theta)}{2k^2}\left[(\frac{\partial u}{\partial\rho})^2 - \frac{\ell^2 u^2}{\rho^2}\right]\cos 2\phi\Bigg\}.\end{aligned} \tag{22}$$

One can see that the on-axis potential consists of a ϕ-independent term (the second term in Eq. (22), which is just an average of the potentials due to two oppositely circularly-polarized light beams) and a ϕ-dependent term (the last term in Eq. (22)). The azimuthal dependence of the last three term in Eq. (22) can be traced back to the expression for the longitudinal field given in Eq. (20) which is seen to be expressible as a superposition of terms containing $e^{i\phi}$ and $e^{-i\phi}$. They can be interpreted as the superposition of the spin-to-orbit longitudinal fields by right- and left-circularly-polarized components of the linearly-polarized light. Thus, the ϕ-dependent set of terms is the result of the interference of these two longitudinal terms.

The potential landscape is displayed in Fig. 4 when linearly-polarised light is used with the parameters the same as those used to generate Fig. 1–3. The crucial on-axis ϕ-dependent contribution to the overall potential was found to be small, so maybe neglected when considering the potential for the bottle trap.

For the more general case, where the polarization of the beam is intermediate between the two circular polarizations of opposite helicity ($\sigma = \pm 1$), it is straightforward to show that the

Optics EXPRESS

trapping potential evolves with the ellipticity of the light in a non-trivial manner. As in the linear polarization case, it consists of the sum of a ϕ-independent contribution defined by the relative potential of the two oppositely circularly-polarized light and a ϕ-dependent term defined by the interference of the longitudinal components and whose importance is maximized for the linearly-polarized case. As the azimuthal contribution is small even for the linear polarization case, we can expect the axial trapping potential to be linearly tunable from a maximum when $\sigma = -1$ to zero when $\sigma = 1$, both with $\ell = 1$. For the beam width we are considering ($w_0 = 0.9\lambda$), the amplitude of the longitudinal field component is still a fraction the magnitude of the transverse field component.

Appendix C: examples of bottle trap characteristics

Table 1. Characteristics of the two adjacent main bottle traps. Each of the four columns in the table concerns a bottle trap set-up with different values of laser power and polarisation (σ). The common parameters are as follows: the atomic transition wavelength λ_0=852.35nm, the detuning = $\Delta = 1.33 \times 10^{15}$ Hz, beam *NA* = 0.35 and the winding number $\ell = 1$. By symmetry, the same bottle trap characteristics are reproduced for light beams with $\ell = -1$ and $\sigma = -\ell = 1$ or $\sigma = 0$. $E_{rec} = \hbar^2 k^2/2M$)

Laser Power (mW) (Polarization σ)		0.4 (-1)	1 (-1)	4 (-1)	4 (0)
Central bottle	Ground State Energy (E_{rec})	28	45	90	70
	Saddle Point Potential Barrier Height (E_{rec})	60	180	600	160
	Saddle Point *Tunnelling Rate* (Hz)	0.038	$7\text{x}10^{-7}$	10^{-15}	10^{-5}
	Axial *Tunnelling Rate* (Hz)	0.0017	10^{-8}	10^{-20}	$6 \text{ x } 10^{-8}$
	Radial *Spring Constant* $K_{\rho,0}$ (N/m)	$9 \text{ x } 10^{-15}$	$2 \text{ x } 10^{-14}$	$9 \text{ x } 10^{-14}$	$5 \text{ x } 10^{-14}$
	Axial *Spring Constant* $K_{z,0}$ (N/m)	$2 \text{ x } 10^{-14}$	$6 \text{ x } 10^{-14}$	$2 \text{ x } 10^{-13}$	$3 \text{ x } 10^{-14}$
Nearest neighbour bottle	Ground State Energy (E_{rec})	25	40	79	61
	Saddle Point Potential Barrier Height (E_{rec})	50	149	500	100
	Saddle Point *Tunnelling Rate* (Hz)	0.092	$2 \text{ x } 10^{-5}$	$5 \text{ x } 10^{-13}$	$4 \text{ x } 10^{-4}$
	Axial *Tunnelling Rate* (Hz)	0.65	$7 \text{ x } 10^{-8}$	$4 \text{ x } 10^{-15}$	$3 \text{ x } 10^{-5}$
	Radial *Spring Constant* $K_{\rho,1}$ (N/m)	$7 \text{ x } 10^{-15}$	$2 \text{ x } 10^{-14}$	$7 \text{ x } 10^{-14}$	$7 \text{ x } 10^{-14}$
	Axial *Spring Constant* $K_{z,1}$ (N/m)	$2 \text{ x } 10^{-14}$	$5 \text{ x } 10^{-14}$	$2 \text{ x } 10^{-13}$	$5 \text{ x } 10^{-14}$

Optics EXPRESS

Table 2. Characteristics of the two adjacent main bottle traps if laser beams are focused using a lens. Each of the three columns concerns a bottle trap set-up with different values of the Numerical Aperture (NA) of the lens. The common parameters are as follows: the atomic transition wavelength λ_0=852.35nm, the detuning = $\Delta = 1.33 \times 10^{15}$ Hz and the winding number $\ell = 1$. By symmetry, the same bottle trap characteristics are reproduced for light beams with $\ell = -1$ and $\sigma = -\ell = 1$. The laser power is fixed at 4mW. $E_{rec} = \hbar^2 k^2 / 2M$)

Beam Width ($w_0(\lambda)$) (NA)		1.3 (0.25)	1.1 (0.30)	0.9 (0.35)
Central bottle	Ground State Energy (E_{rec})	48	67	90
	Saddle Point Potential Barrier Height (E_{rec})	200	350	600
	Saddle Point *Tunnelling Rate* (Hz)	7×10^{-7}	2×10^{-11}	10^{-15}
	Axial *Tunnelling Rate* (Hz)	7×10^{-9}	2×10^{-14}	10^{-20}
	Radial *Spring Constant* $K_{\rho,0}$ (N/m)	2×10^{-14}	5×10^{-14}	9×10^{-14}
	Axial *Spring Constant* $K_{z,0}$ (N/m)	8×10^{-14}	1×10^{-13}	2×10^{-13}
Nearest neighbour bottle	Ground State Energy (E_{rec})	41	60	79
	Saddle Point Potential Barrier Height (E_{rec})	180	400	500
	Saddle Point *Tunnelling Rate* (Hz)	0.001	3×10^{-12}	5×10^{-13}
	Axial *Tunnelling Rate* (Hz)	3×10^{-8}	3×10^{-15}	4×10^{-15}
	Radial *Spring Constant* $K_{\rho,1}$ (N/m)	2×10^{-14}	4×10^{-14}	7×10^{-14}
	Axial *Spring Constant* $K_{z,1}$ (N/m)	5×10^{-14}	1×10^{-13}	2×10^{-13}

Acknowledgments. The support of University of York's York Open Access Fund for publication under Creative Commons Attribution (CC BY) licence is greatly appreciated.

Disclosures. The authors declare no conflicts of interest.

Data availability. No data were generated or analyzed in the presented research.

References

1. L. Allen, M. W. Beijersbergen, R. J. C. Spreeuw, *et al.*, "Orbital Angular Momentum of Light and the Transformation of Laguerre-Gaussian Laser Modes," Phys. Rev. A **45**(11), 8185–8189 (1992).
2. J. Götte and S. Barnett, "Light Beams Carrying Orbital Angular Momentum," in *The Angular Momentum of Light*, D. L. Andrews and M. Babiker, eds., (Cambridge University Press, 2012), pp. 1–27.
3. O. Jones, P. H. Maragó, and G. Volpe, *Optical Tweezers: Principles and Applications* (Cambridge University Press, 2015).
4. G. Li, P. Zhang, and T. Zhang, "Three-dimensional Cooling of a Single Atom by a Pair of Counter-propagating Tightly Focused Beams," Opt. Express **23**(18), 23571–23581 (2015).
5. T. Kuga, Y. Torii, N. Shiokawa, *et al.*, "Novel Optical Trap of Atoms with a Doughnut Beam," Phys. Rev. Lett. **78**(25), 4713–4716 (1997).
6. N. B. Simpson, K. Dholakia, L. Allen, *et al.*, "Mechanical Equivalence of Spin and Orbital Angular Momentum of Light: an Optical Spanner," Opt. Lett. **22**(1), 52–54 (1997).
7. M. J. Snadden, A. S. Bell, R. B. M. Clarke, *et al.*, "Doughnut Mode Magneto-optical Trap," J. Opt. Soc. Am. B **14**(3), 544 (1997).
8. Y. Torii, N. Shiokawa, T. Hirano, *et al.*, "Pulsed Polarization Gradient Cooling in an Optical Dipole Trap with a Laguerre-Gaussian Laser Beam," Eur. Phys. J. D **1**(3), 239–242 (1998).
9. D. P. Rhodes, D. M. Gherardi, J. Livesey, *et al.*, "Atom Guiding Along High Order Laguerre–Gaussian Light Beams Formed by Spatial Light Modulation," J. Mod. Opt. **53**(4), 547–556 (2006).
10. A. Kennedy, G. W. Biedermann, J. T. Farrar, *et al.*, "Confinement of Ultracold Atoms in a Laguerre–Gaussian Laser Beam Created With Diffractive Optics," Opt. Commun. **321**, 110–115 (2014).

Optics EXPRESS

11. M. Babiker, D. L. Andrews, and V. E. Lembessis, "Atoms in Complex Twisted Light," J. Opt. **21**(1), 013001 (2018).
12. S. H. Kazemi, M. Veisi, and M. Mahmoudi, "Atom Localization Using Laguerre–Gaussian Beams," J. Opt. **21**(2), 025401 (2019).
13. M. D Al-Amri, D. L. Andrews, and M. Babiker, eds., Structured Light for Optical Communications (Elsevier: Cambridge MA, 2021).
14. S. Franke-Arnold, J. Leach, M. J. Padgett, *et al.*, "Optical Ferris Wheel for Ultracold Atoms," Opt. Express **15**(14), 8619–8625 (2007).
15. A. A. Rsheed, A. Lyras, V. E. Lembessis, *et al.*, "Guiding of Atoms in Helical Optical Potential Structures," J. Phys. B **49**(12), 125002 (2016).
16. J. Arlt and M. J. Padgett, "Generation of a Beam with a Dark Focus Surrounded by Regions of Higher Intensity: the Optical Bottle Beam," Opt. Lett. **25**(4), 191–193 (2000).
17. L. Isenhower, W. Williams, A. Dally, *et al.*, "Atom Trapping in an Interferometrically Generated Bottle Beam Trap," Opt. Lett. **34**(8), 1159–1161 (2009).
18. P. Xu, X. He, J. Wang, *et al.*, "Trapping a Single Atom in a Blue Detuned Optical Bottle Beam Trap," Opt. Lett. **35**(13), 2164–2166 (2010).
19. A. S. Arnold, "Extending Dark Optical Trapping Geometries," Opt. Lett. **37**(13), 2505–2507 (2012).
20. O. Aldossary, "Bottle Atom Trapping Configuration by Optical Dipole Forces," J. King Saud Univ. Sci. **26**(1), 29–35 (2014).
21. G. Li, S. Zhang, L. Isenhower, *et al.*, "Crossed Vortex Bottle Beam Trap for Single-Atom Qubits," Opt. Lett. **37**(5), 851–853 (2012).
22. D. Barredo, V. Lienhard, P. Scholl, *et al.*, "Three-dimensional Trapping of Individual Rydberg Atoms in Ponderomotive Bottle Beam Traps," Phys. Rev. Lett. **124**(2), 023201 (2020).
23. Y. Xiao, Z. Yu, R. A. Wambold, *et al.*, "Efficient Generation of Optical Bottle Beams," Nanophotonics **10**(11), 2893–2901 (2021).
24. K. Y. Bliokh and F. Nori, "Transverse and Longitudinal Angular Momenta of Light," Phys. Rep. **592**, 1–38 (2015).
25. G. F. Quinteiro, F. Schmidt-Kaler, and C. T. Schmiegelow, "Twisted-Light-Ion Interaction: The Role of Longitudinal Fields," Phys. Rev. Lett. **119**(25), 253203 (2017).
26. P. Wozniak, I. D. Leon, K. Höflich, *et al.*, "Interaction of Light Carrying Orbital Angular Momentum with a Chiral Dipolar Scatter," Optica **6**(8), 961 (2019).
27. K. Forbes, D. Green, and G. Jones, "Relevance of Longitudinal Fields of Paraxial; Optical Vortices," J. Opt. **23**(7), 075401 (2021).
28. V. E. Lembessis, K. Koksal, J. Yuan, *et al.*, "Chirality-enabled Optical Dipole Potential Energy for Two-level Atoms," Phys. Rev. A **103**(1), 013106 (2021).
29. L. Allen, M. Padgett, and M. Babiker, "IV The Orbital Angular Momentum of Light," in *Progress in Optics*, vol. 39 (Institute of Physics, 1999), pp. 291–372.
30. S. M. Barnett and R. Zambrini, *Orbital Angular Momentum of Light* (Springer New York, 2007), pp. 277–311.
31. Y. Zhao, J. S. Edgar, G. D. M. Jeffries, *et al.*, "Spin-to-orbital Angular Momentum Conversion in a Strongly Focused Optical Beam," Phys. Rev. Lett. **99**(7), 073901 (2007).
32. P. van der Straten and H. Metcalf, *Atoms and Molecules Interacting with Light: Atomic Physics for the Laser Era* (Cambridge University Press, 2016).
33. D. L. Andrews and M. Babiker, eds., *The Angular Momentum of Light* (Cambridge University Press, 2012).
34. D. Jaksch, C. Bruder, J. I. Cirac, *et al.*, "Cold Bosonic Atoms in Optical Lattices," Phys. Rev. Lett. **81**(15), 3108–3111 (1998).
35. V. E. Lembessis, A. Lyras, and O. M. Aldossary, "Optical Ferris Wheels as a Platform for Collisional Quantum Gates," J. Opt. Soc. Am. B **38**(1), 233–240 (2021).
36. C. Cohen-Tannoudji and D. Guery-Odelin, *Advances in Atomic Physics: An Overview* (World Scientific, p. 166, 2011).
37. O. Mandel, M. Greiner, A. Widera, *et al.*, "Coherent Transport of Neutral Atoms in Spin-dependent Optical Lattice Potentials," Phys. Rev. Lett. **91**(1), 010407 (2003).
38. F.-R. Winkelmann, C. A. Weidner, G. Ramola, *et al.*, "Direct Measurement of the Wigner Function of Atoms in an Optical Trap," J. Phys. B **55**(19), 194004 (2022).
39. D. L. Haycock, S. E. Hamann, G. Klose, *et al.*, "Atom-trapping in the Lamb-Dicke Regime in a Far-off-resonance Optical Lattice," in *Atom Optics*, vol. 2995 M. G. Prentiss and W. D. Phillips, eds., International Society for Optics and Photonics (SPIE, 1997), pp. 163–172.
40. X. Zhang, W. Fu, J. Lv, *et al.*, "Multiple Bottle Beams Based on Metasurface Optical Field Modulation and Their Capture of Multiple Atoms," Chin. Phys. B **31**(8), 088103 (2022).
41. Y. Zhou and M. Hong, "Formation of a Three-dimensional Bottle Beam via an Engineered Microsphere," Photonics Res. **9**(8), 1598 (2021).
42. O. Minin, W. Chen, S. Chien, *et al.*, "In-plane Subwavelength Optical Capsule for Lab-on-a-chip Nano-tweezers," Opt. Lett. **47**(4), 794 (2022).

Optics EXPRESS

43. R. Ramos, D. Spierings, I. Racicot, *et al.*, "Measurement of the Time Spent by a Tunnelling Atom within the Barrier Region," Nature **583**(7817), 529–532 (2020).
44. P. Meystre, *Atom Optics* (Springer: New York, 2001).
45. S. Altshuler, L. M. Frantz, and R. Braunstein, "Reflection of Atoms from Standing Light Waves," Phys. Rev. Lett. **17**(5), 231–232 (1966).
46. H. Batelaan, "The Kapitza-Dirac Effect," Contemp. Phys. **41**(6), 369–381 (2000).